Hindawi
International Journal of RF and Microwave Computer-Aided Engineering
Volume 2023, Article ID 7855907, 12 pages
https://doi.org/10.1155/2023/7855907

Research Article

Design and Analysis of a Low-Profile Dual-Band Circularly Polarized Monopole Antenna Based on Characteristic Mode Analysis

Kingsford Sarkodie Obeng Kwakye,[1] Nouman Rasool,[2] Kwame Oteng Gyasi,[1] Joseph Abroquah,[1] Mubarak Sani Ellis,[1] Ohemeng Lord Owusu,[1] Abdul-Rahman Ahmed,[1] and Jerry John Kponyo[1]

[1]*Department of Telecommunication Engineering, Kwame Nkrumah University of Science and Technology, Ghana*
[2]*School of Electronic and Information Engineering, Electromagnetic Technology and Engineering Key Laboratory, China West Normal University, Nanchong, Sichuan, China*

Correspondence should be addressed to Nouman Rasool; engr_nouman77@yahoo.com

Received 11 April 2023; Revised 10 September 2023; Accepted 19 September 2023; Published 7 October 2023

Academic Editor: Lu Guo

This paper presents the design of a simple dual-band circularly polarized monopole antenna using characteristic mode analysis. First, a dual-band elliptically polarized "L"-shaped monopole antenna with a partial ground is designed; then, a rectangular stub and a parasitic structure on the ground plane are implemented to achieve dual-band CP operation. To enhance impedance bandwidth and generate circular polarization in the upper band, the rectangular stub is attached to the "L"-shaped strip. The parasitic structure is employed for simultaneous dual-band CP radiation. Characteristic mode analysis is undertaken to predict the performance of the antenna before excitation. The modal analysis which is undertaken before excitation shows the natural modes that can be excited by the antenna structure to generate a dual-band CP response. The analysis gives approximate bandwidths that can be achieved by the antenna even before excitation. The overall dimension of the antenna is $0.379\lambda_0 \times 0.379\lambda_0 \times 0.015\lambda_0$, where λ_0 is the corresponding free-space wavelength at 5.7 GHz. The measured -10 dB impedance bandwidth (ZBW) is realized to be 75.9% (4.5 GHz–10 GHz). The measured 3 dB axial ratio bandwidths (ARBW) at the lower and upper bands are 6% (5.6 GHz–5.95 GHz) and 28% (6.65 GHz–8.82 GHz), respectively. The proposed antenna features a simple and compact structure for Wi-Fi, WLAN, WiMAX, and C band applications.

1. Introduction

In recent years, circularly polarized (CP) antennas have received a lot of attention because they possess a number of significant advantages over linearly polarized (LP) antennas. With CP antennas, the "Faraday rotation" effect caused by the ionosphere is greatly reduced. When LP signals are used, the Faraday rotation effect produces a significant signal loss (around 3 dB or more) [1–21]. Also, CP antennas do not require the need for transmitting (Tx) and receiving (Rx) antennas to have the same orientation, and the received signal strength remains relatively constant. This differs from LP antennas, which suffer polarization mismatch losses if the Tx and Rx antennas are misaligned. Moreover, CP antennas are effective against multipath interference and fading.

Characteristic modal analysis on antennas and conducting bodies is fast becoming an area of interest in the electromagnetics, antennas, and propagation community [21–28]. A set of orthogonal real currents on the surface of a conducting body is represented by characteristic modes. These modes are independent of the applied excitation and are simply dependent on the size and shape of the structure.

This detail is particularly relevant to the antenna designer as it serves to cut down the cost of time and work needed in the antenna optimization process [23].

Compact CP antennas with multiband functionality have attracted a lot of interest due to the rapid proliferation of wireless communication in radio frequency identification [2, 3], mobile communication [4], navigation satellite systems [5, 6], wireless local area networks (WLAN) [7, 8], and 5G systems that require high-gain, low-profile, and wideband CP antennas [18–21]. A complementary semicircle-shaped monopole antenna is used to achieve LP dual-band operation [9]. To achieve circular polarization, rectangular and L-shaped adjusting stubs are added. The antenna proposed in [9] suffers from narrow bandwidths of 1.66% and 11.9% in the lower and upper bands, respectively, in addition to a relatively large size. By exciting four compact dual-band inverted-F monopoles with a 90° phase offset sequential feeding network, circular polarization is achieved [5]. However, the design may suffer from complicated structures. A modified ground including three slots, including a T-shaped and two inverted-L topologies is designed to achieve circular polarization with a bent feeding structure in [10]. The proposed structure however possesses a narrow bandwidths of 4.14% and 4.59% and a large size. A simple monopole with two rectangular parasitic elements and an I-shaped grounded stub is used to obtain dual-band CP simultaneously albeit with a large area of $0.64\lambda^2$, where λ is the free-space wavelength at the center frequency of the lower band [11]. To accomplish dual-band operation with good impedance matching and circular polarization performance, a radiator patch with a "C"-shaped strip for the higher band and an "L"-shaped strip for the lower band is employed [12]. Two circular eccentric rings (CECRs) with different sizes, each working as a single-band circular polarization radiator, are simultaneously excited by an arc-shaped strip to achieve dual-band circular polarization [13]. In [14], two deformed parallel monopoles with a crane-shaped strip as a perturbation element are used to excite a compact dual-band CP with a small frequency ratio. The antennas designed in [12–14] have drawbacks of obtaining a narrow bandwidths less than 12% in both bands in addition to having large overall sizes, whereas the authors in [15] employ the use of multiple feed to achieve dual-wideband CP by combining slot and monopole modes at the expense of possessing a very large antenna. CMA has been employed for the design and analysis of CP antennas but mostly restricted to broadband antennas with there being a paucity in the use of CMA for the design of multiband CP antennas [25–29]. Also, it can be seen from the prior discussion that currently existing antennas possess either a complex structure with a large size or narrow bandwidths which make them not favourable for implementation in current wireless devices.

In this article, a low-profile single fed dual-band CP monopole antenna for C band applications is presented. The main contribution of this paper is that it achieves a dual-band CP with a simple and compact antenna design. Also, the use of CMA to predict the performance of the antenna provides the antenna research community with an efficient way to design and optimize antennas. The antenna consists of a parasitic structure, rectangular stub, partial ground, and an "L"-shaped microstrip radiator. The rectangular stub is optimized to enable the antenna radiate CP waves. Dual-band CP operation is achieved by using a parasitic strip. The designed antenna has a simple structure with a total area of $0.14\lambda^2$ and achieves very competitive fractional CP bandwidths of 6% and 28% with peak gains of 1.7 dBi and 1.9 dBi, respectively, in the lower and upper bands. The simple design structure makes the proposed antenna a very suitable starting design for CP antennas of various configurations.

2. Antenna Design and Analysis

2.1. Antenna Configuration. The antenna is printed on a low-cost FR4 substrate with a dielectric constant of 4.4 and dielectric loss tangent, $tan\boldsymbol{d}$, of 0.02. Considering a low-profile antenna design, the antenna has a height of 0.8 mm and an overall size of 20 mm × 20 mm × 0.8 mm. Numerical driven simulations were executed with the commercial ANSYS High-Frequency Structure Simulator (HFSS ver. 21) software. The geometry of the proposed dual-band CP monopole antenna is shown in Figure 1, and the optimized parameters are listed in Table 1. The proposed antenna has on top of the substrate an impedance transformer of width 0.5 mm and length of 1.5 mm which matches the 50 Ω microstrip feedline to the "t"-shaped patch. The ground plane consists of partial ground and a parasitic structure. The size of the partial ground is 20 mm × 5 mm.

2.2. Antenna Evolution. The development stages of the proposed antenna are illustrated in three steps as described by Ant 1–Ant 3 in Figure 2. Ant 1–Ant 3 are used to explain the antenna evolution with the help of characteristic mode analysis. It is worth noting that the CMA simulations in this section were undertaken with the CST numerical software.

Real current modes known as characteristic modes are numerically obtained for conducting objects with arbitrary shapes [25]. These modes are the conductor's naturally existing currents; hence, they are not affected by the applied excitation but rather the conductor's size and form. The total current density on the conductor can be expressed as follows [23]:

$$J = \sum_n \alpha_n J_n, \tag{1}$$

where J_n represents the nth current mode and a_n is the modal weighting coefficient (MWC) which tells how much the nth mode contributes to the total current after excitation. This modal weighting coefficient can be calculated as follows [23]:

$$\alpha_n = \frac{V_n'}{1 + j\lambda_n}, \tag{2}$$

where V_n is referred to as to as the modal excitation coefficient (MEC) which represents the coupling between each mode and the applied external excitation [7] and λ_n

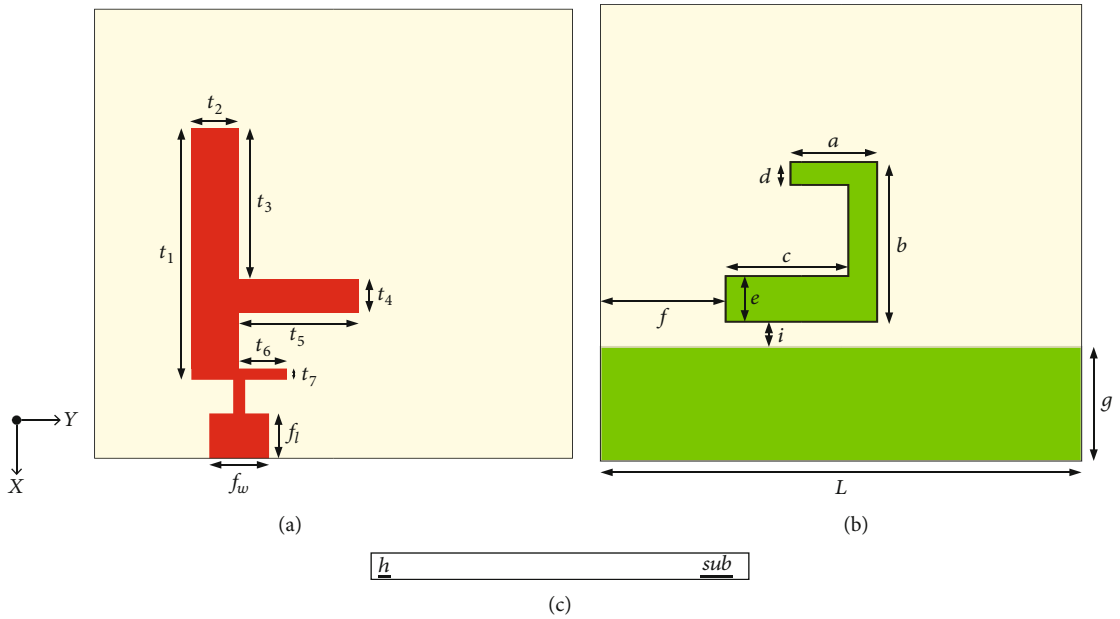

Figure 1: Geometry of the designed antenna. (a) Front view, (b) Back view, (c) Side view.

Table 1: Dimensions of the designed antenna (unit: millimetres).

Parameter	Value	Parameter	Value	Parameter	Value	Parameter	Value	Parameter	Value
a	3.6	b	7	c	5.1	d	1	e	2
f	5.2	g	5	h	0.8	i	1.1	l	20
f_w	2.5	f_l	2	t_1	11.2	t_2	2	t_3	6.7
t_4	1.5	t_5	5	t_6	2	t_7	0.5		

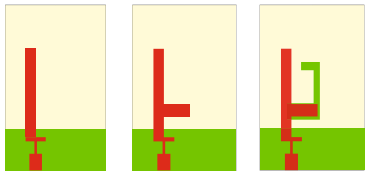

Figure 2: Development stages of the proposed antenna.

represents the eigenvalue associated with the nth mode which gives information about how well a mode will potentially contribute to radiation after excitation. Zero eigenvalue ($\lambda = 0$) modes represent modes that are potentially resonant and that would contribute well to radiation, whereas modes with eigenvalues not equal to zero contribute either to the storage of electric energy (negative eigenvalues) or magnetic energy (positive eigenvalue) [23].

The theory of characteristic modes (TCM) has been considerably derived for various antenna configurations in the open literature. TCM borders on numerous concepts; however, for circularly polarized antennas, two parameters are generally considered when analysing with TCM, namely, modal significance (MS) and characteristic angle (CA) both as functions of eigenvalue. The MS and CA have been significantly studied in [23] and are thus not discussed in-depth in this paper for brevity. The CA and MS can be derived as follows:

$$\mathrm{CA} = 180 \circ -\tan^{-1}\lambda_n, \tag{3}$$

$$\mathrm{MS} = \left|\frac{1}{1 + j\lambda_n}\right|. \tag{4}$$

It is observed from (3) and (4) that, ideally, resonance is representative of MS equal to 1 and CA equal to 180° [25]. It is widely known in the antenna research community that for CP to be generated, two orthogonal modes with equal amplitudes have to be excited [17]. For CMA, the requirements for CP to be realized are that two resonant modes having the same modal significance and a characteristic angle difference of ideally 90° at the frequency of interest be excited. A modal significance ≥ 0.7 is generally acceptable as a threshold for resonant modes. Also, the two modes for CP should have CAs above and below 180° (ideally 225° and 135°), respectively, to account for the 90° CA difference. The CAs are required to be above and below 180° to ensure that the combined modes resonate (i.e., capacitive and inductive modes cancel out). Moreover, both modes must attain identical directivities at the radiation angle of interest in addition to having orthogonal current distributions [26].

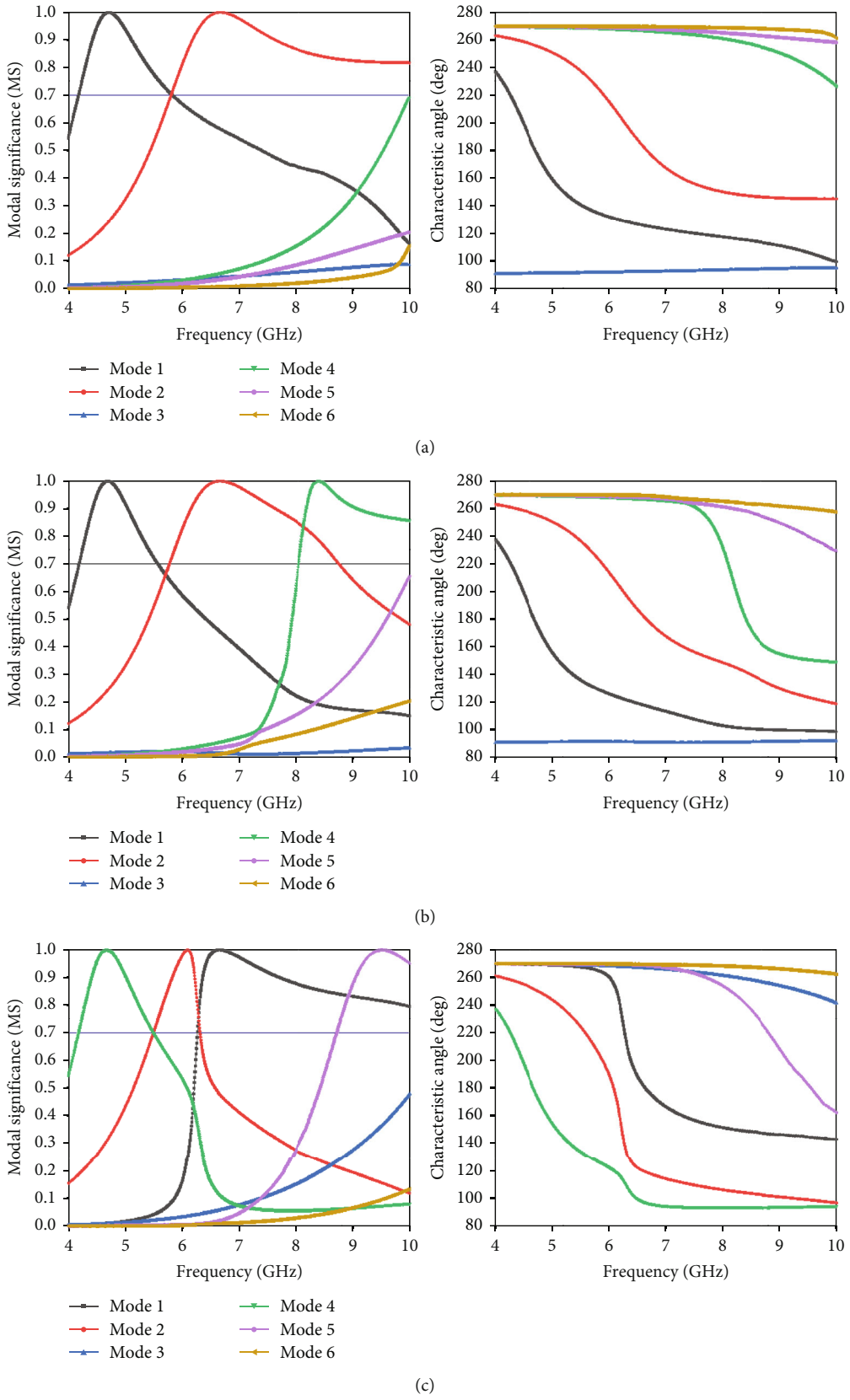

Figure 3: Modal significance and characteristic angle plots for the first 6 modes: (a) Ant 1; (b) Ant 2; (c) Ant 3.

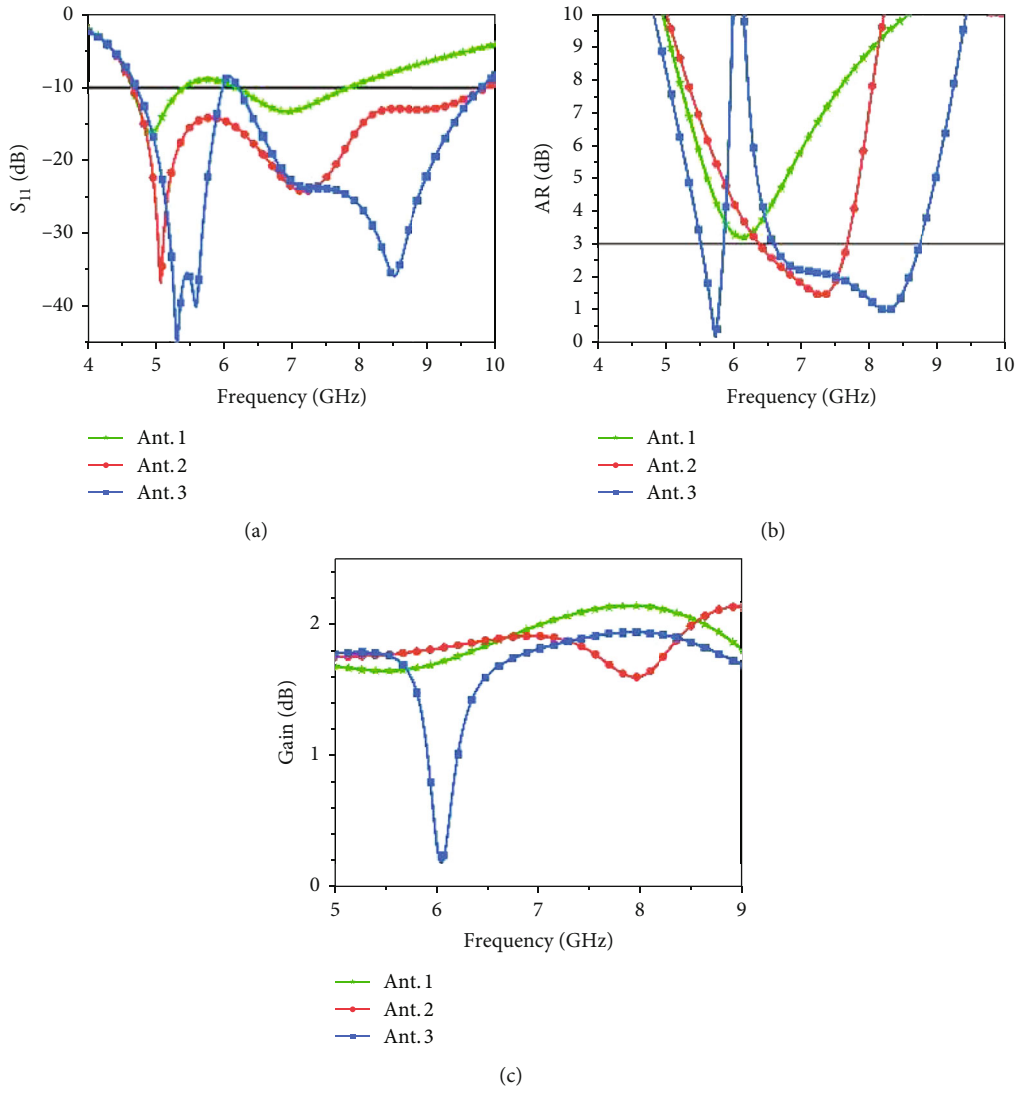

FIGURE 4: Simulated results of Ant 1–Ant 3. (a) S_{11}; (b) AR; (c) gain.

The MS and CA are used in the following section to describe the evolution of the antenna design. It is worth mentioning that the MS and CA provide information about the radiating capability of a mode, while the MWC depicts excitation of a mode as a result of the source [26].

Ant 1 as seen in Figure 2 consists of a simple "L"-shaped patch on top of the substrate and a partial rectangular ground at the bottom of the substrate. It is realized from the MS plot in Figure 3(a) that modes 1 and 2 are dominant and intersect around 5.8 GHz with an MS of 0.7 and a CA difference of ~85°. This is expected to generate a narrowband CP response around 5.8 GHz after excitation. These two modes are also expected to generate two resonances around 4.8 GHz and 6.8 GHz as seen from the MS plot. As observed from the AR plot after excitation in Figure 4(b), Ant 1 does not achieve an AR below 3 dB around 5.8 GHz but is seen to possess an AR very close to 3 dB. This discrepancy between the CMA and excited structure can be attributed to the fact that the MEC is introduced after excitation and can hence affect the predicted performance [28]. Also, it can be deduced from the closeness of the CMA and excited antenna results that a slight adjustment of the monopole structure can potentially lead to the AR falling below 3 dB. It is also realized from Figure 4(a) that Ant 1 generates two operating bands with -10 dB impedance bandwidths of 764 MHz and 1667 MHz in the lower (around 4.8 GHz) and upper bands (around 6.8 GHz), respectively, after excitation. It is again realized from the S_{11} plot that even though the two modes that generate these resonances have an MS of 1, the S_{11} values are not very good. This goes to show that the excitation of the modes can be further improved.

By protruding a rectangular strip of the size 5 mm ×1.5 mm from the stem of the L-strip to form a "t-shaped" monopole antenna as illustrated in Ant 2, it is observed from Figure 3(b) that mode 4 becomes a dominant mode, and this is thus expected to enhance the impedance bandwidth. It can also be observed from the MS plot that modes 1 and 2 intersect below 0.7 at 5.72 GHz but have a CA difference of 97° whereas modes 2 and 4 intersect at 8.15 GHz with an MS of 0.82 and a CA difference of 68°. These results predict a weak CP response

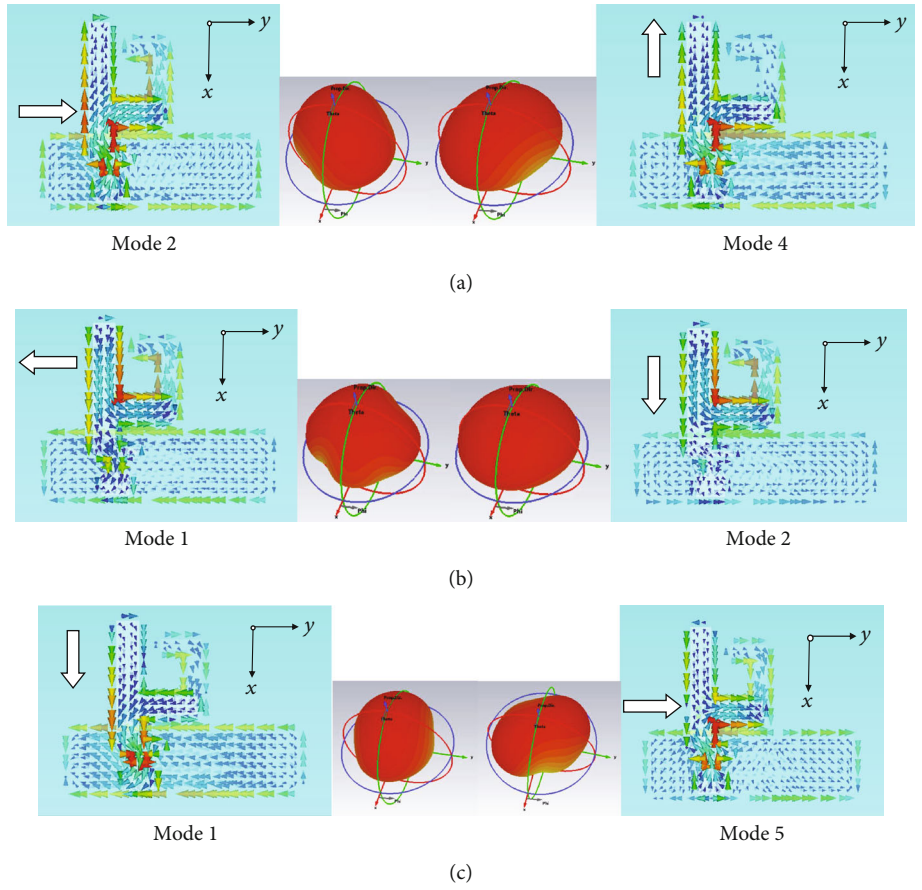

FIGURE 5: Far field radiation pattern and current distributions of orthogonal modes at (a) 5.5 GHz, (b) 6.3 GHz, and (c) 8.9 GHz.

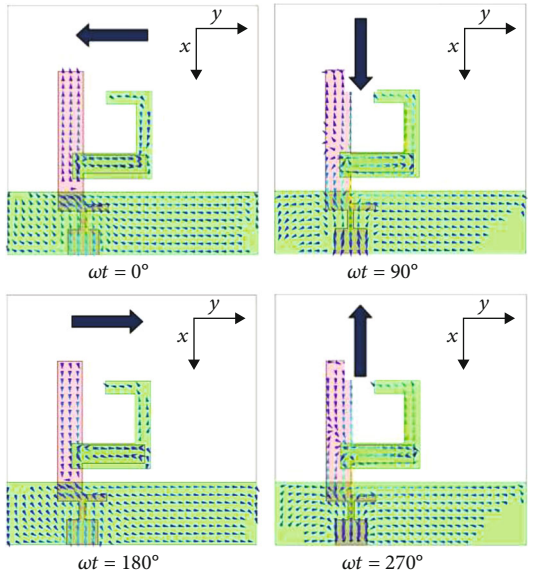

FIGURE 6: Time-varying surface current distribution of the proposed antenna at 5.8 GHz different angular times.

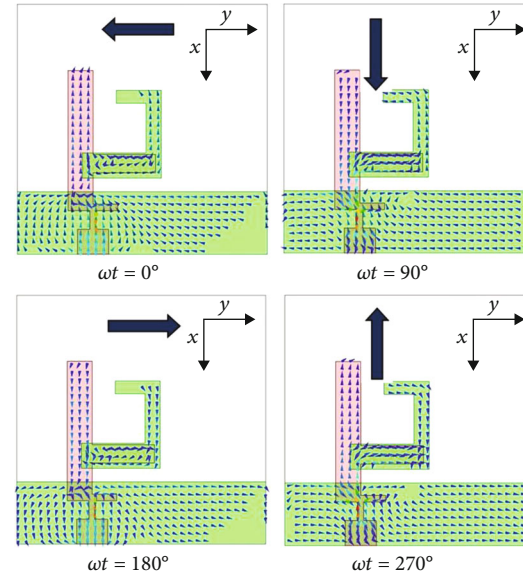

FIGURE 7: Time-varying surface current distribution of the proposed antenna at 7.2 GHz at different angular times.

around 5.72 GHz (due to the low MS) and an elliptical (near circular) polarization response around 8.15 GHz (due to the CA difference being 68°). Since mode 2 contributes to the potential generation of CP at both 5.72 GHz and 8.15 GHz, it is expected that a "weak" broadband CP will be generated between 5.72 GHz and 8.15 GHz. Upon exciting antenna 2, it

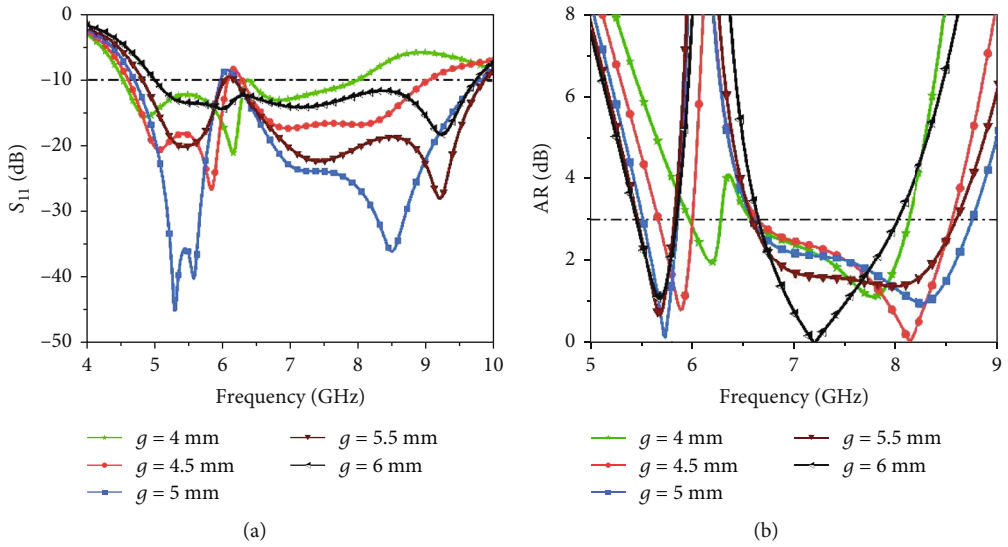

Figure 8: Effect of g on (a) S_{11} and (b) AR.

is realized that a wide ZBW of 4.65 GHz–9.87 GHz with an ARBW of 6.3 GHz-7.7 GHz is achieved. It is realized that the broadband S_{11} is achieved as predicted. In fact, it can be seen that the original resonances from Ant 1 have been improved which can be attributed to the MEC doing a better job at coupling the modes to the applied excitation. It is observed that the near CP response and weak CP radiation prediction result in CP performances albeit with slight displacements from the predicted frequencies. This can be attributed again to the improvement in the MEC as already mentioned. This shows that a better feed structure can be employed to achieve a wider ARBW with the configuration of Ant 2 [29].

Ant 3, which is the final structure, consists of Ant 2's configuration in addition to a parasitic structure that is etched at the bottom of the substrate. As observed from the MS plot in Figure 3(c), modes 1, 2, 4, and 5 are the dominant modes due to their MS being equal to 1 at different frequencies across the band of interest. It can be observed that the MS of modes 2 and 4 is 0.7 at 5.5 GHz and the CA difference between the two modes at 5.5 GHz is ~90°. Modes 1 and 2 can also be seen to have their MS intersecting with a value of 0.8 at 6.3 GHz with a CA difference of ~98°. Finally, modes 1 and 5 have an MS of 0.82 at 8.9 GHz with a CA difference of about 70°. The current distribution and patterns are studied for antenna 3 in Figure 5. It is realized that all the pairs of modes mentioned above have similar directivities and orthogonal current distributions at the frequencies where their MSs intersect. At 6.3 GHz, it is realized that both the vertical and horizontal currents on the ground plane for mode 2 cancel out leaving just the monopole and parasitic patch currents as the dominant ones that lead to radiation. For mode 1, it can be seen that the horizontal currents on the ground plane contribute constructively to the antenna radiation, thereby showing an orthogonality in the dominant current distributions. This analysis depicts a narrow CP bandwidth resulting from the contribution of modes 2 and 4 (which can be observed to be narrowband modes from the MS plot) around 5.5 GHz. A broad CP bandwidth that ranges from 6.3 GHz to 8.9 GHz as a result of the contributions from the pair of modes 1 and 2 and modes 1 and 5, respectively, is also realized in addition to the narrow band. The broadband nature is mainly attributed to mode 1 which is a broadband mode. Comparing this to the simulated results after excitation, it is realized that the results are in very good agreement, i.e., 5.52-5.8 GHz and 6.6-8.75 GHz after excitation and a narrow 5.5 GHz band with a 6.3–8.9 GHz band before excitation using CMA. The discrepancies between the CMA and excited antenna results are attributed to the effects of the applied excitation which as explained previously is not considered during the calculation of the MS and CA responses [28]. This analysis shows the power of CMA in the design of CP antennas.

2.3. CP Mechanism. Figures 6 and 7 show the time-varying surface current distribution for the four-phase angles of 0°, 90°, 180°, and 270° at 5.8 GHz and 7.21 GHz, respectively. The arrow indicates the direction of the dominant surface current. As shown in Figures 6 and 7, the current on the parasitic structure and the partial ground contributes significantly to the antenna radiation. When the phase is 0°, the dominant surface current points towards $-y$ whereas at $\omega t = 90\circ$, the surface current along $+x$ direction dominates. We observe that the surface current distribution at 180° and 270° is equal in magnitude but opposite in direction to phases of 0° and 90°. As time varies, the predominant surface current flows in the anticlockwise direction in the azimuth plane. Hence, RHCP waves in the boresight direction ($+z$) can be excited in both bands.

3. Numerical Analysis for the Antenna

A parametric study to obtain the optimized parameters in Table 1 is undertaken in this section. When a parameter is studied, all other parameters are kept at their optimized values. Effects of parameters g, e, a, and t_3 on S_{11} and axial ratio are studied. These parameters are chosen to show the

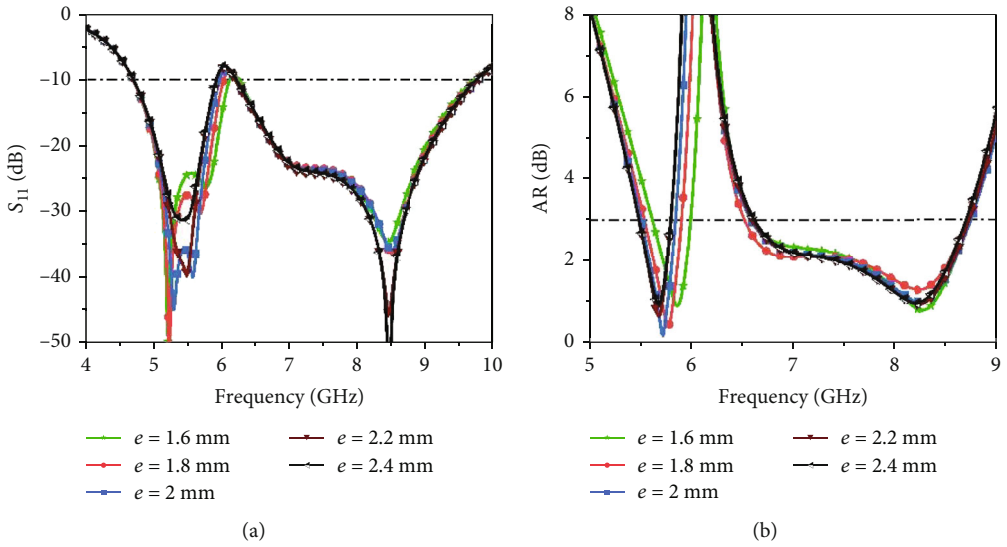

Figure 9: Effect of e on (a) S_{11} and (b) AR.

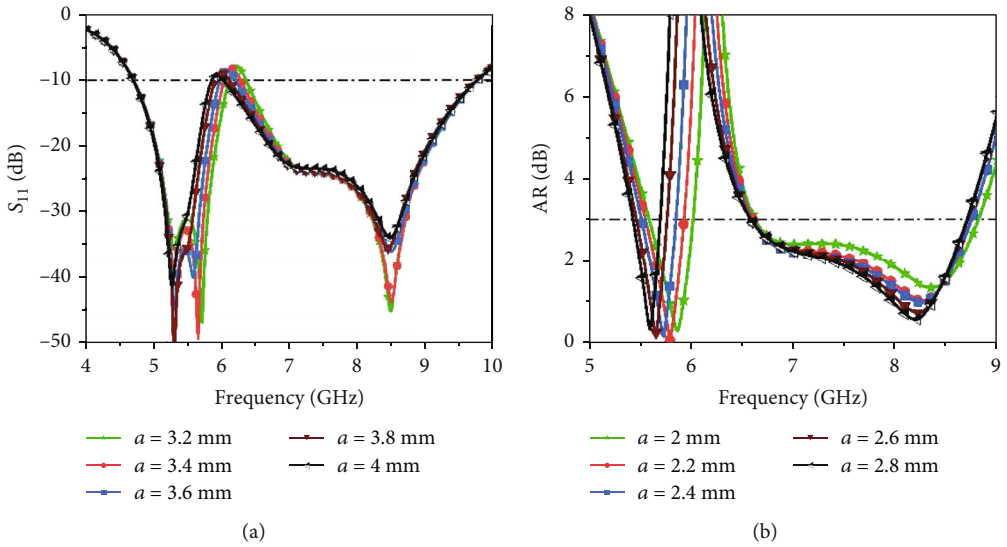

Figure 10: Effect of a on (a) S_{11} and (b) AR.

effect each component (ground plane (g), monopole (t_3), and parasitic patch (e, a)) has on the antenna performance. Figure 8 shows the effect of g on antenna performance. It has a significant effect on axial ratio and S_{11}. The significant effect is attributed to the fact that the ground plane of compact planar antenna plays a vital role in the radiation characteristics. This effect has been studied and utilized for a number of antenna designs including generation of CP [30]. Also, from the current distribution analysis of Ant 3 in the CMA section, it is realized that the currents on the ground plane play a major role on the antenna performance. It can be seen from Figure 8(a) that as g is varied from 4 mm to 5 mm, the impedance bandwidth improves in the upper band but deteriorates in the lower band albeit with an improvement in the S_{11} values. As g is increased from 5 mm to 6 mm, it is observed that the S_{11} values deteriorate in both bands. From Figure 8(b), it is seen that when g is increased, ARBW is enhanced in both bands up until $g = 5$ mm, after which it is observed to deteriorate. For wider ZBW and ARBW as well as better impedance matching, g is chosen to be 5 mm.

The effect of e on S_{11} and AR is shown in Figure 9. As e increases, it is observed in Figure 9(a) that impedance matching is slightly improved in both bands whereas in Figure 9(b), the resonant AR frequency for the lower band decreases. This shows that e can be used to tune the CP performance in the lower frequency band without adversely affecting the upper band. The optimal value of e is chosen as 2 mm.

The influence of a on S_{11} and axial ratio is shown in Figure 10. In Figure 10(b), the lower band shifts to the left and the purity of circular polarization is improved slightly

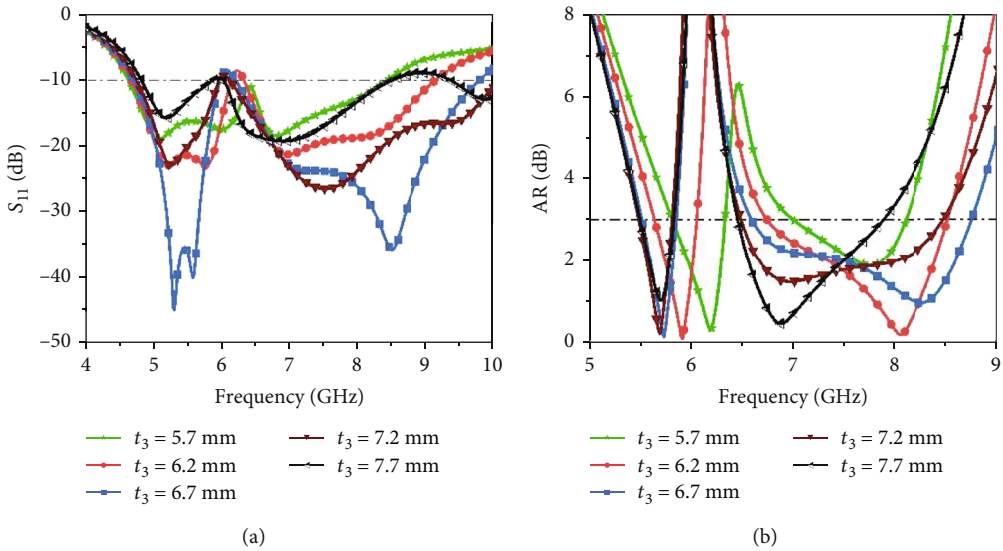

FIGURE 11: Effect of t_3 on (a) S_{11} and (b) AR.

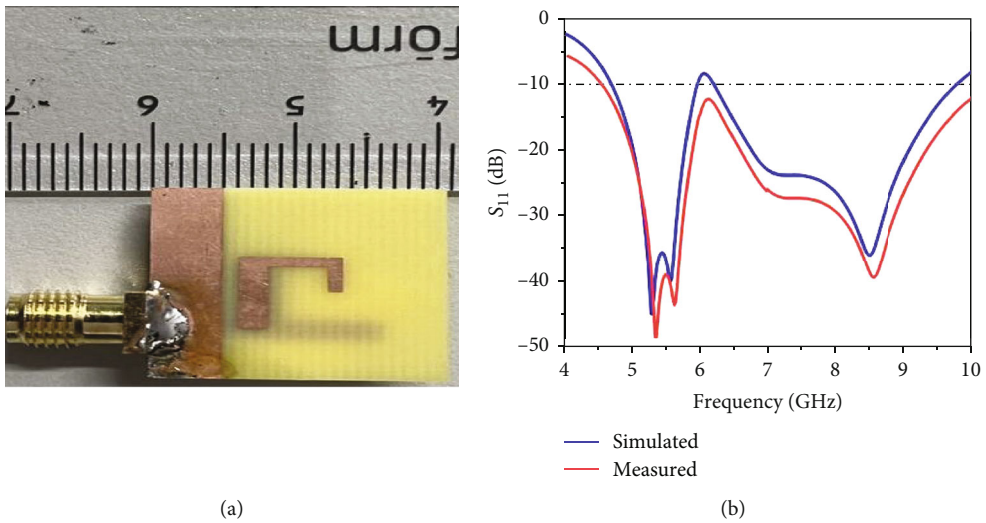

FIGURE 12: (a) Photograph of the proposed antenna. (b) Simulated and measured S_{11}.

in the upper band. As shown in Figure 10(a), increasing the length of a slightly improves the bandwidth in the upper frequency band whiles slightly deteriorating the bandwidth in the lower frequency range. It can be seen that a can be used to tune the lower CP band based on the frequency range of interest. An optimal value of a is chosen to be 3.6 mm for the proposed antenna.

Figure 11 illustrates the simulation results of S_{11} and AR with change in t_3. This parameter is expected to have adverse effects on both the S_{11} and ARBW as it forms part of the main radiator. Also, from the CMA section, it is realized that the stub plays a major role in the excitation of the antenna as observed from its effect in Ant 2. As shown in Figure 11(b), as t_3 increases, lower band is seen to have its AR bandwidth reducing and moving toward the lower frequency range. However, it is observed that the AR bandwidth in the upper frequency band improves till $t_3 = 7.2$ mm, after which it begins to worsen. The impedance bandwidth is seen to improve as the length is increased from 5.7 mm to 6.7 mm after which it begins to deteriorate. This can be attributed to the fact that increasing the length increases the inductance of the antenna leading to poorer matching as the length increases beyond 7.2 mm. For dual-band CP operation with better impedance matching as well as wide ARBW, t_3 is set to 6.7 mm.

4. Results and Discussion

Prototype of the proposed dual-band CP antenna is shown in Figure 12(a). Figure 12(b) illustrates the simulated and measured -10 dB impedance bandwidth. The S_{11} was measured using a Rohde & Schwarz (ZNB 40) Vector Network Analyzer whereas the far field parameters were measured in an anechoic chamber. The discrepancy between the

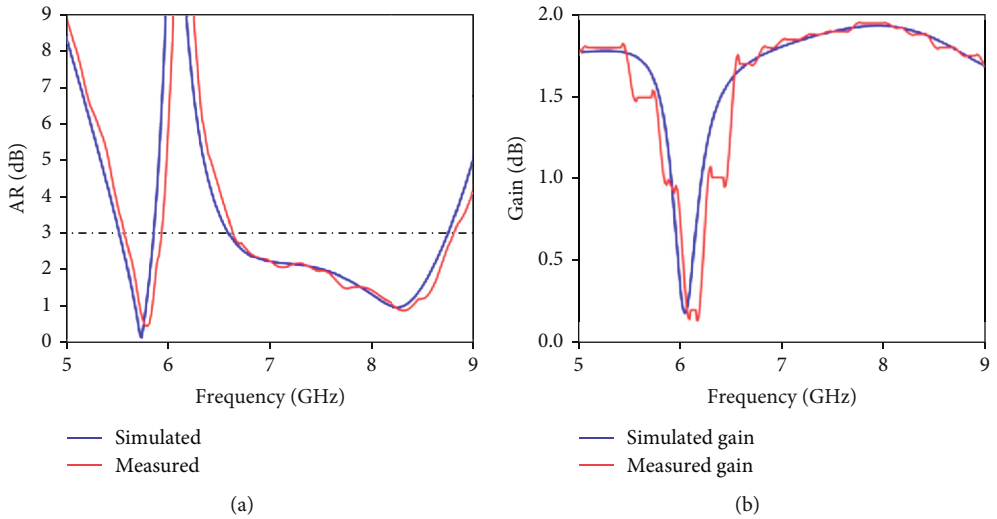

Figure 13: Simulated and measured (a) axial ratio and (b) gain.

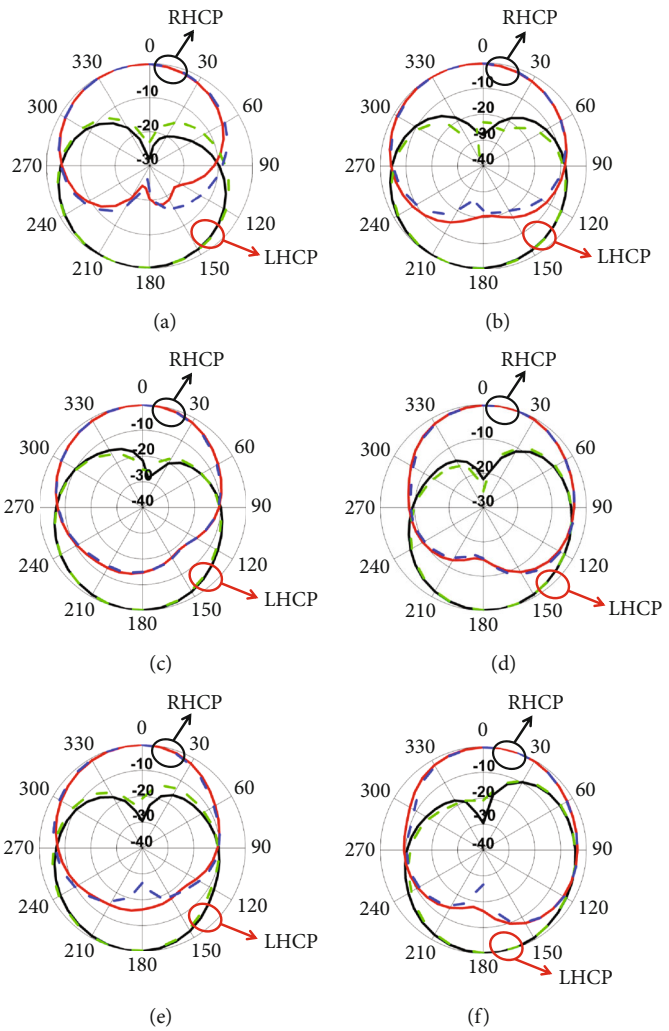

Figure 14: Simulated (solid) and measured (dashed) radiation pattern at 5.7 GHz in the (a) *xz* and (b) *yz* planes, at 7.5 GHz in the (c) *xz* and (d) *yz* planes, and at 8 GHz in the (e) *xz* and (f) *yz* planes.

Table 2: Comparison between referenced antenna and proposed antenna.

Reference	Overlapped lower band (GHz) %	Overlapped upper band (GHz) %	Overall size (mm^3)	Gain (dBi)
[3]	0.902–0.928, 2.84	2.40–2.48, 3.28	$0.2\lambda_0 \times 0.2\lambda_0 \times 0.02\lambda_0$	-0.60, 1.2
[5]	1.236–1.286, 4.2	1.532–1.572, 2.6	$0.211\lambda_0 \times 0.211\lambda_0 \times 0.057\lambda_0$	3.4, 2.9
[8]	2.27–2.52, 10.5	5.14–5.47, 6.56	$0.493\lambda_0 \times 0.554\lambda_0 \times 0.0197\lambda_0$	2.4, 2.8
[9]	2.39-2.43, 1.66	5.06-5.70, 11.9	$0.56\lambda_0 \times 0.40\lambda_0 \times 0.0107\lambda_0$	2.0, 4.5
[10]	1.538–1.603, 4.14	2.28–2.384, 4.59	$0.458\lambda_0 \times 0.550\lambda_0 \times 0.0147\lambda_0$	4.3
[11]	2.2–2.9, 27.45	3.40–3.65, 7.1	$0.735\lambda_0 \times 0.875\lambda_0 \times 0.0187\lambda_0$	2.5
[12]	2.39–2.57, 7.3	5.213–6.0, 16	$0.600\lambda_0 \times 0.705\lambda_0 \times 0.0225\lambda_0$	2.48, 3.09
[13]	2.096–2.105, 0.4	3.59–3.61, 0.6	$0.665\lambda_0 \times 0.665\lambda_0 \times 0.0285\lambda_0$	8.4, 9.9
[14]	1.47–1.61, 9	1.87–2.09, 11	$0.42\lambda_0 \times 0.42\lambda_0 \times 0.010\lambda_0$	4.0
[15]	1.17–2.5, 72.5	3.52–6.26, 56	$1.13\lambda_0 \times 1.25\lambda_0 \times 0.0125\lambda_0$	4.0, 3.05
[16]	2.48–2.56, 4.76	3.48–3.63, 4.21	$0.74\lambda_0 \times 0.70\lambda_0 \times 0.030\lambda_0$	6.52, 7.04
Proposed	5.62–5.95, 6	6.65–8.82, 28	$0.379\lambda_0 \times 0.379\lambda_0 \times 0.015\lambda_0$	1.7, 1.9

simulated and measured result which is most significant with the S_{11} results is caused by errors arising from fabrication and calibration of the VNA during measurement. The simulated and measured axial ratio and gain versus frequency are shown in Figures 13(a) and 13(b). The measured -10 dB impedance bandwidth (ZBW) is observed to be 75.9% (4.5 GHz–10 GHz), respectively. The measured 3 dB axial ratio bandwidths (ARBW) at the lower and upper bands are 6% (5.62 GHz–5.95 GHz) and 28% (6.65 GHz–8.82 GHz), respectively. This is observed to be in very good agreement with the simulated overlapping CP bandwidth of 5.52 GHz–5.86 GHz and 6.6 GHz–8.75 GHz. It is also seen that the antenna achieves a peak gain of 1.7 dBi and 1.9 dBi in the lower and upper bands, respectively. The axial ratio and gains are measured in the broadside direction (phi = theta = 0 ∘). The low gain values are attributed to the compactness and bidirectional nature of the monopole antenna. To improve it, techniques like the employment of a back reflector [17] or the use of metasurface structures [18–21] can be adopted. The perturbations in the gain plot are mainly attributed to the effect of the RF cable employed during the far field anechoic chamber measurement process. The simulated and measured CP radiation patterns at 5.7 GHz, 7.5 GHz, and 8 GHz are shown in Figure 14. RHCP which is the co-pol component is realized in the $+z$ direction, whereas LHCP which is the cross-pol component is in the $-z$ direction.

A comparison between the proposed antenna and formerly published works is shown in Table 2. λ_0 is the corresponding free-space wavelength at the center frequency of the overlapped lower band. The proposed antenna has the advantage of low-profile and wide overlapped ZBW and ARBW as observed from the table. It is realized that the proposed antenna suffers from a low gain, but this can be solved with the implementation of a back reflector [17] or a metasurface structure [18–21].

5. Conclusion

A compact, dual-band t-shaped CP monopole antenna with a parasitic strip has been presented. Characteristic mode analysis has been employed to exhibit that the t-shaped monopole in addition to a very simple parasitic strip can generate dual-band circular polarization. The proposed antenna which has a compact size of $20 \times 20 \times 0.8\,mm^3$ has been fabricated and measured. The proposed antenna achieves competitive measured overlapping S_{11} and 3 dB axial ratio bandwidths of 6% (5.6 GHz–5.95 GHz) and 28% (6.65 GHz–8.82 GHz), respectively, at the lower and upper bands. The designed antenna also achieves peak gains of 1.7 and 1.9 dBi in the lower and upper bands, respectively, with bidirectional patterns in both bands. The proposed antenna provides a compact size, simple design structure, broadband CP performance, and moderate gains as compared to most of the existing dual-band CP monopole antennas. The proposed antenna could be used for Wi-Fi, WLAN, WiMAX, and C band applications.

Data Availability

The data used to support the findings of this study are available from the corresponding author upon request.

Conflicts of Interest

The authors declare no conflict of interest.

Acknowledgments

This work was supported by the Doctoral Research Funding of China West Normal University (Grant Number: 21E022).

References

[1] S. Gao, Q. Luo, and F. Zhu, *Circularly Polarized Antennas*, Wiley, Hoboken, NJ, USA, 2014.

[2] R. Xu, J. Liu, K. Wei et al., "Dual-band circularly polarized antenna with two pairs of crossed-dipoles for RFID reader," *IEEE Transactions on Antennas and Propagation*, vol. 69, no. 12, pp. 8194–8203, 2021.

[3] R. Caso, A. Michel, M. Rodriguez-Pino, and P. Nepa, "Dual-band UHF-RFID/WLAN circularly polarized antenna for

portable RFID readers," *IEEE Transactions on Antennas and Propagation*, vol. 62, no. 5, pp. 2822–2826, 2014.

[4] S. Sadeghi-marasht, M. S. Sharawi, and A. Zhu, "Dual-band circularly polarized antenna array for 5G millimeter-wave applications," *IEEE Open Journal of Antennas and Propagation*, vol. 3, pp. 314–323, 2022.

[5] C. Li, F. S. Zhang, F. Zhang, and K. Yang, "A compact dual-band circularly polarized antenna with wide HPBWs for CNSS applications," *International Journal of Antennas and Propagation*, vol. 2018, Article ID 3563949, 10 pages, 2018.

[6] R. Xu, S. S. Gao, J. Liu et al., "Analysis and design of ultrawideband circularly polarized antenna and array," *IEEE Transactions on Antennas and Propagation*, vol. 68, no. 12, pp. 7842–7853, 2020.

[7] D. Fazal and Q. U. Khan, "Dual-band dual-polarized patch antenna using characteristic mode analysis," *IEEE Transactions on Antennas and Propagation*, vol. 70, no. 3, article 22712276, 2022.

[8] J. H. Lu and C. W. Liou, "Planar dual-band circular polarization monopole antenna for wireless local area networks," *IEEE Antennas and Wireless Propagation Letters*, vol. 14, pp. 478–481, 2015.

[9] W. Liang, Y. Jiao, Y. Luan, and C. Tian, "A dual-band circularly polarized complementary antenna," *IEEE Antennas and Wireless Propagation Letters*, vol. 14, pp. 1153–1156, 2015.

[10] C. J. Wang, M. H. Shih, and L. T. Chen, "A wideband open-slot antenna with dual-band circular polarization," *IEEE Antennas and Wireless Propagation Letters*, vol. 14, pp. 1306–1309, 2015.

[11] R. K. Saini, S. Dwari, M. K. Mandal, and S. Member, "CPW-fed dual-band dual-sense circularly polarized monopole antenna," *IEEE Antennas and Wireless Propagation Letters*, vol. 16, pp. 2497–2500, 2017.

[12] M. Tan and B. Wang, "A dual-band circularly polarized planar monopole antenna for WLAN / Wi-Fi applications," *IEEE Antennas and Wireless Propagation Letters*, vol. 15, pp. 670–673, 2016.

[13] Z. X. Liang, D. C. Yang, X. C. Wei, and E. P. Li, "Dual-band dual circularly polarized microstrip antenna with two eccentric rings and an arc-shaped conducting strip," *IEEE Antennas and Wireless Propagation Letters*, vol. 15, pp. 834–837, 2016.

[14] C. Chen and E. K. N. Yung, "Dual-band circularly-polarized CPW-fed slot antenna with a small frequency ratio and wide bandwidths," *IEEE Transactions on Antennas and Propagation*, vol. 59, no. 4, pp. 1379–1384, 2011.

[15] R. Xu, J. Y. Li, J. Liu, S. G. Zhou, Z. J. Xing, and K. Wei, "A design of dual-wideband planar printed antenna for circular polarization diversity by combining slot and monopole modes," *IEEE Transactions on Antennas and Propagation*, vol. 66, no. 8, pp. 4326–4331, 2018.

[16] K. Li, L. Li, Y. Cai, C. Zhu, and C. Liang, "A novel design of low-profile dual-band circularly polarized antenna with meta-surface," *IEEE Antennas and Wireless Propagation Letters*, vol. 14, pp. 1650–1653, 2015.

[17] K. Oteng Gyasi, G. J. Wen, D. Inserra et al., "A compact broadband cross-shaped circularly polarized planar monopole antenna with a ground plane extension," *IEEE Antennand as and Wireless Propagation Letters*, vol. 17, no. 2, pp. 335–338, 2018.

[18] J. Wang, J. Zhao, Y. Cheng, H. Luo, and F. Chen, "Dual-band high-gain microstrip antenna with a reflective focusing metasurface for linear and circular polarizations," *AEU - International Journal of Electronics and Communications*, vol. 157, article 154413, 2022.

[19] T. Shi, R. Chai, X. Chen, M. Li, T. Zhang, and M. -C. Tang, "A low-profile, circularly polarized, metasurface-based antenna with enhanced bandwidth and stable high gain," *IEEE Antennas and Wireless Propagation Letters*, vol. 22, no. 2, pp. 253–257, 2023.

[20] J. Wang, Y. Cheng, H. Luo, F. Chen, and L. Wu, "High-gain bidirectional radiative circularly polarized antenna based on focusing metasurface," *AEU - International Journal of Electronics and Communications*, vol. 151, article 154222, 2022.

[21] C. Huang, C. -J. Guo, Y. Yuan, and J. Ding, "Dual-band dual-sense high-gain circularly polarized metasurface antenna using characteristic mode analysis," *IEEE Antennas and Wireless Propagation Letters*, vol. 22, no. 1, pp. 154–158, 2023.

[22] Z. Zhang, Y. Cheng, H. Luo, and F. Chen, "Low-profile wideband circular polarization metasurface antenna with characteristic mode analysis and mode suppression," *IEEE Antennas and Wireless Propagation Letters*, vol. 22, no. 4, pp. 898–902, 2023.

[23] M. Cabedo-Fabres, E. Antonino-Daviu, A. Valero-Nogueira, and M. FerrandoBataller, "The theory of characteristic modes revisited: a contribution to the design of antennas for modern applications," *IEEE Antennas and Propagation Magazine*, vol. 49, no. 5, pp. 52–68, 2007.

[24] K. Y. Kabalan, A. El-Hajj, and R. F. Harrington, "Characteristic mode analysis of a slot in a conducting plane separating different media," *IEEE Transactions on Antennas and Propagation*, vol. 38, no. 4, pp. 476–481, 1990.

[25] K. Oteng Gyasi, A. Boukarkar, K. S. Obeng Kwakye et al., "Characteristic mode analysis of a compact circularly polarized rotated square slot antenna," *Microwave and Optical Technology Letters*, vol. 65, no. 6, pp. 1762–1769, 2023.

[26] H. H. Tran, N. Nguyen-Trong, and A. M. Abbosh, "Simple design procedure of a broadband circularly polarized slot monopole antenna assisted by characteristic mode analysis," *IEEE Access*, vol. 6, pp. 78386–78393, 2018.

[27] Y. Chen and C.-F. Wang, *Characteristic Modes: Theory and Applications in Antenna Engineering*, Wiley, 2015.

[28] M. S. Ellis, N. A. Owusu-Achiaw, S. A. Osei, and D. Nakojah, "Circularly polarized edge-placed printed monopole antenna using theory of characteristic modes," *Microwave and Optical Technology Letters*, vol. 65, no. 8, pp. 2314–2322, 2023.

[29] A. El Yousfi, A. Lamkaddem, K. A. Abdalmalak, and D. Segovia-Vargas, "A broadband circularly polarized single-layer metasurface antenna using characteristic-mode analysis," *IEEE Transactions on Antennas and Propagation*, vol. 71, no. 4, pp. 3114–3122, 2023.

[30] L. Zhang, Y.-C. Jiao, Y. Ding, B. Chen, and Z.-B. Weng, "CPW-fed broadband circularly polarized planar monopole antenna with improved ground-plane structure," *IEEE Transactions on Antennas and Propagation*, vol. 61, no. 9, pp. 4824–4828, 2013.